C.P. No. 1197

MINISTRY OF DEFENCE (PROCUREMENT EXECUTIVE)

AERONAUTICAL RESEARCH COUNCIL

CURRENT PAPERS

Flow in a Supersonic Jet expanding from a Convergent Nozzle

By

J. C. Gibbings, J. Ingham and D. Johnson

Fluid Mechanics Division,

University of Liverpool

LONDON: HER MAJESTY'S STATIONERY OFFICE

1972

Price 60p net

CP No. 1197≠
July, 1968

FLOW IN A SUPERSONIC JET EXPANDING FROM A CONVERGENT NOZZLE

- By -
J. C. Gibbings, J. Ingham* and D. Johnson+,
Fluid Mechanics Division,
University of Liverpool

SUMMARY

Various characteristics of a very uniform sonic jet of air that expands into a stationary atmosphere are determined experimentally and compared with a simple analysis and with existing analytical results. Comparison of the analysis is made with existing results of characteristic calculations.

1. Introduction

This report describes an investigation into the flow field of an axi-symmetric jet expanding from a circular convergent nozzle into a stationary atmosphere.

An early analytical study of this flow was made by Prandtl (Ref.1). It was based upon a model of a jet which was formed by small perturbation from a parallel and constant area flow. It was thus limited to values of the ratio of the jet outlet pressure, p_j, to the atmospheric pressure p_a, that were above but near to unity. For larger values of this pressure ratio many solutions have been obtained using the method of characteristics (Ref.2). Further studies have resulted in the presentation of relations that approximately express the results of the characteristics calculations (Ref.3).

All these analytical studies have excluded the effects of viscous mixing though the characteristics solutions have taken account of the presence of shock waves within the jet flow.

The previous experimental studies that have been reported were largely based upon optical methods (Ref.4). Some quantities, such as the diameter of the jet, are difficult to determine from schlieren observation and other characteristics, such as the quality of the jet flow at outlet, cannot be assessed. Interferometric studies have been used to obtain the variation of density throughout the jet (Ref.5) but when this is the only property measured a complete description of the flow is not possible. Descriptions of pitot tube and static tube traverse measurements have been given (Ref.6). In some cases the accuracy of these traverse measurements has been limited by the small size of the jet in comparison with that of the probes. Also difficulties in using probes near to the shock waves in the jet have been reported (Ref.4).

In/

≠Replaces A.R.C.30 371

*Now at Modern Metals (Fagley) Ltd.

+Now at Admiralty Research Laboratory, Teddington

In the work described here traverses were made by pitot and static tubes in a jet that issued from a nozzle with a high degree of uniformity at the nozzle outlet.

2. The Nozzle Design and Flow

The convergent nozzle that was used is illustrated in Fig.1. It was profile machined to a template that was made to conform closely to the ordinates of the two-dimensional contraction shape tabulated in Ref.7; the two-dimensional contraction ratio of 3.0 giving an area contraction through the circular nozzle of 9:1. The last 0.3 in of the nozzle at outlet was machined at a constant diameter of 0.5077 in and care was taken to remove any burrs at the outlet edge without rounding it. The outlet face of the nozzle was machined to be perpendicular to the nozzle axis, thus providing means of setting the traverse axis parallel to the nozzle axis and enabling the optical path for the schlieren and shadowgraph systems to be set perpendicularly to the nozzle axis.

At the upstream end of the nozzle two 32 mesh by 32 standard wire gauge wire gauzes were fixed across the pipe as shown in Fig.1. A further 12 diameters upstream from these gauzes a third one of 16 mesh by 16 standard wire gauge was fixed in a position just downstream of the control valve system.

Pressures were measured by liquid manometers or by Bourdon type gauges. The latter were frequently calibrated against an air operated dead-weight tester.

As a result of the care in design and manufacture of this apparatus the flow at outlet from the nozzle was very uniform. This is illustrated by the results of a pitot-tube traverse for a choked nozzle flow, that is shown in Fig.2. The variation in pitot-pressure, p_1, is seen to be symmetrical about the axis and the total variation is only 0.075% of the upstream static pressure, p_o.

3. Results of Shadowgraph Observations

The cellular structure of an expanding jet contains repetitions of either an olique shock system as shown in the sketch above Fig.3 or it contains repetitions of a mixed oblique, normal shock system with a Mach intersection as sketched in Fig.6. In either case a viscous mixing region at the edge of the jet reduces the radial extent of these patterns with successive celluar repetitions.

To observe these patterns a shadowgraph optical system was set up with great care, a second schlieren mirror being used to obtain a focussed image of approximately twice full size.

The upper curve of Fig.3. shows the results of measurements, from a shadowgraph picture, of the distance to the ends of the successive cells. The end of the cell was taken as that position where the reflected shock met the boundary of the circular jet, a position shown by a line, on the shadowgraph picture, perpendicular to the jet axis. The cells are seen to get progressively longer up to the third one; the fourth to the seventh

are all of the same length, successively the eighth onwards are of a common but now smaller length. Prandtl's analysis (Ref.1) gives the positions of the ends of successive cells as being proportional to the rooths of $J_o(x) = 0$ where $J_o(x)$ is the Bessel function of the first kind of zero order. Differences of these roots are then proportional to the cell lengths, and values are plotted, as a ratio of the first root which is proportional to the first cell length, as squared points are indicated by a chain line in Fig.4. Also plotted are the measured cell lengths again as a ratio of the measured length of the first cell. Within the experimental scatter the trend of an observed increase in cell length up to the third cell followed by cells of constant length is seen to be predicted by Prandtl's analysis, though the latter gives numerical values generally above the experimental ones.

There was never any evidence from the shadowgraph observations, at any point within the range of pressures used in all the present tests, that the jet axis was other than straight and parallel to the nozzle axis. A careful traverse with a pitot-tube along a line perpendicular to the nozzle axis and 20 diameters downstream of the nozzle outlet gave a jet axis that was approximately 0.004 in. from the nozzle axis. This was within the accuracy of the plug gauge used to determine the nozzle axis. This result is in contrast to the lack of symmetry at some pressure ratios that was observed by Love et al (Ref.2). It may be that their jet flow was influenced by the straight sided shape of the nozzle that they used.

The lower curve of Fig.3 shows the way in which the distances between successive shock intersections on the jet axis varied from cell to cell. These variations are seen to be markedly similar to those for the cell lengths.

Fig.5 illustrates the result of measurements, from a shadowgraph picture, of the width of successive joints between cells. This width is seen to decrease linearly from cell to cell, a result in marked contrast to the previously described variation in the cell lengths.

As the ratio between the jet stagnation pressure and the surrounding atmosphere, p_s/p_a, is increased beyond a certain value, the oblique shock intersection on the axis of the first cell changes to a normal shock Mach intersection (Ref.2). To determine this bounding pressure ratio the width of the Mach shock was measured from the shadowgraph observations. Values are plotted against pressure ratio in Fig.6. An extrapolation to zero width gives the dividing pressure ratio as,

$$\frac{p_s}{p_a} - 1.893 = 1.58$$

or

$$\frac{p_s}{p_a} = 3.47.$$

The results are replotted on log-log scales in Fig.7 where they are seen to fit a straight line variation. This line is given by,

$$\frac{w_1}{d_j} = \left[0.25 \frac{p_s}{p_a} - 3.47\right]^{0.86}$$

The position, within the first cell, of the intersection of the shock with the jet axis varies with the pressure ratio. The observed positions are shown plotted in Fig.8. The results are seen to fit two straight line relations, the dividing point being given by the previously determined pressure ratio at which the width of the Mach shock becomes zero.

For an oblique shock intersection, at $\left(\frac{p_s}{p_a} - 1.893\right) < 1.58$, the fitted line is given by

$$\frac{\ell_1}{d_j} = 0.76 \left[\frac{p_s}{p_a} - 1.893\right]^{0.61}$$

For a Mach shock intersection, at $\left(\frac{p_s}{p_a} - 1.893\right) > 1.58$, the fitted line is given by,

$$\frac{\ell_1}{d_j} = 0.84 \left[\frac{p_s}{p_a} - 1.893\right]^{0.415} \qquad \ldots(1)$$

Some authors have expressed their results for the Mach shock position in the form (Refs.8, 9);

$$\frac{\ell_1}{d_j} \propto \left[\frac{p_s}{p_j}\right]^n$$

which for values of the pressure ratio such that $\frac{p_s}{p_a} >> 1.893$ is of the form of equation (1) used to fit the present results. Crist et al (Ref.9) have obtained experimental results that fit

$$\frac{\ell_1}{d_j} = 0.68 \left(\frac{p_s}{p_a}\right)^{0.49}$$

Values given by this relation are shown as the chain line in Fig.8. They do not agree with the present results. However, as D'attorre and Harshbarger (Ref.8) have pointed out, their results fit,

$$\frac{\ell_1}{d_j} \propto \left[\frac{p_j}{p_a}\right]^{\frac{1}{2}}$$

when conical nozzles are used and fit

$$\frac{\ell_1}{d_j} \propto \left[\frac{p_j}{p_a}\right]^{\frac{5}{6}}$$

when contoured nozzles are used. So the discrepancy just noted again may be due to differences in design of the nozzles.

No sign could be seen on the shadowgraph pictures of a second shock wave on the axis at a closer position to the nozzle outlet. Such a shock was observed by Love et al (Ref.2). In their case it may have been a consequence of the use of a conical shape for the nozzle (Ref.10).

A means of estimating the position of the Mach shock has been proposed (Ref.11). It is based on the assumption that the pressure on the axis behind the normal shock is equal to that of the atmosphere surrounding the jet. Calculations using this method give the results represented by the dotted line in Fig.8. Agreement is seen to be poor at the lower end of the Mach shock regime, and at the upper end this calculated curve is seen to cross the experimental one as was shown by Adamson (Ref.4).†

At the dividing point between the region of oblique shock intersection and that of Mach shock it is seen that $\ell_1/d_j = 1.00$. In the absence of the shock, that is at a higher value of p_s/p_a, the Mach number at this position was carefully measured to be 2.545 (Ref.12). A normal shock wave at this position would have a downstream Mach number, M_2, of 0.508 and correspondingly $p_2/p_o = 0.402$. In comparison, with this Mach number of 2.545 upstream of an oblique shock reflected as another having a maximum deflection, the downstream Mach number is 0.92 and $p_2/p_o = 0.458$. Thus this latter case is not the criterion for the onset of a Mach shock, and shadowgraph observation showed that at this bounding condition the shock intersection shape was as illustrated in Fig.9. This shows that an oblique shock intersection did not occur but that the upstream shock was rounded and concave forward on the axis. Beyond the region drawn in Fig.9. the adjacent shock system gave, to the accuracy observable, straight lines on the shadowgraph pictures.

In Fig.10 the observed length of the first cell is shown plotted against the pressure ratio. Again the results fit two straight line relations, the dividing point corresponding to the point of onset of a Mach Wave. For the regime corresponding to the oblique shock intersection the curve shown can be represented by,

$$\frac{\ell_2}{d_j} = 1.16\left(\frac{p_s}{p_a} - 1.893\right)^{0.55}$$

---

† The corresponding analysis by Crist et al (Ref.9) gave a curve lower by about 27%

and for the region of Mach shock the curve is given by,

$$\frac{\ell_2}{d_j} = 1.33 \left(\frac{p_s}{p_a} - 1.893 \right)^{0.26}$$

Now, at the dividing point, $\ell_2/d_j = 1.50$.

The first of these relations is comparable with an empirical relation given by Love et al (Ref.2) which is equivalent to

$$\frac{\ell_2}{d_j} = 1.13 \left(\frac{p_s}{p_a} - 1.893 \right)^{\frac{1}{2}}$$

The differences are probably due to the differences in nozzle contour noted earlier.

An analytical solution giving the value of ℓ_2/d_j was obtained by Prandtl as (Ref.1);

$$\frac{\ell_2}{d_j} = 1.2 \left(\frac{p_s}{p_a} - 1.893 \right)^{\frac{1}{2}}$$

Values given by this solution are shown as the upper, dotted curve of Fig.10. This analysis was based upon the assumption of small perturbations about a parallel uniform jet. However, Fig.10 shows that the difference from the experimental values is greater for the lowest pressure ratios where the perturbations would be smallest. Better agreement is obtained at higher pressure ratios and in particular the analytical curve passes through the dividing point of $p_s/p_a = 3.47$, $\ell_2/d_j = 1.50$. The theory of Prandtl was refined by Pack (Ref.13). Results of this latter analysis are shown plotted in Fig.10 as the chain line. In the oblique shock region, compared with Prandtl's solution, that due to Pack gives a curve of lower slope whereas the experiments fall on one of greater slope. Other experimental results (Refs.6, 14) have suggested that Prandlt's relation is valid with modification of the coefficient of 1.2 to a lower value. The present results have shown however that the index of $\frac{1}{2}$ should be slightly higher at 0.55 in the oblique shock range.

The distance to the position of the maximum diameter of the first cell of the jet was not easily determined from the shadowgraph pictures. This is partly because in this region the diameter changes gently and partly because, as will be discussed later, there are marked viscous mixing effects at the boundary of the jet. Results obtained are shown in Fig.11. The lack of precision in locating the position of the maximum diameter is shown by the scatter of the results shown in this Figure. Also plotted in this Figure are the results of calculation, by the method of characteristics, of the jet boundary (Ref.2). Within the large scatter there is agreement between the calculated and experimental results. Tentatively, two straight lines are drawn intersecting, as before, at $p_s/p_a = 3.47$. They are expressed by the relations;

$$\frac{\ell_3}{d_j} = 0.37 \left(\frac{p_s}{p_a} - 1.893 \right)^{1.11}$$

for the oblique shock region, and by,

$$\frac{\ell_3}{d_j} = 0.48 \left(\frac{p_s}{p_a} - 1.893 \right)^{0.48}$$

for the Mach shock region.

4. Results of Pitot and Static Tube Traverses

At axial positions where, from the shadowgraph pictures, it was judged that the jet diameter in the first cell was a maximum, pitot and static tubes were traversed along a line perpendicular to the jet. The distributions of Mach number and pressure obtained are shown plotted for four pressure ratios in Figs.12(a) to (d).

The Mach number distribution shown in Fig.12a has a central isentropic core of almost uniform value out to $y/d_j \simeq 0.2$. At this position there is a rapid drop in Mach number with a corresponding rise in pressure. This position corresponds to the presence of a dark line on the shadowgraph picture which has been described as representing a shock wave. However, the experimental evidence suggests that the compression is gradual and isentropic. Just outside this compression region the measured pressure agrees reasonably with that computed from the pitot traverse which is shown by the dotted line. The discrepancy is possibly due to errors in the static tube reading arising from the presence of gradients in pressure and velocity along the line of traverse and to the flow being at an angle of yaw to the tube. Confirmation that this compression region is not a shock wave is given by the results of interferometer visualisation made by Ladenburg et al (Ref.5). Their results show a distribution of density across this region that has not the sharpness associated with a shock wave. Fig.12(a) also shows that farther out the Mach number decreases towards the isentropic boundary value, then after rising slightly it falls through the outer viscous mixing region.

Figs.12(b), (c) and (d), show that with rising jet pressure the extent of the central core increases, the Mach number fall through the compression region increases, the outer peak in Mach number merges into the outer viscous mixing region and this outer mixing region thickness increases.

5. Mean Mach Number at the Maximum Diameter

From the Mach number distributions shown in Fig.12(a), to (d), mean Mach numbers were computed upon an area basis. These values are shown plotted against the corresponding pressure ratios in Fig.13.

An analysis for the flow in the jet up to the first maximum diameter is given in Appendix I. It supplies a flow solution which is not an isentropic one. Values that it gives for the mean Mach number at the maximum diameter are shown plotted as the solid line in Fig.13. Values for an isentropic solution are shown plotted as the dashed line.

Firstly it is seen that the two analytical solutions are in close agreement down to the pressure ratio of 0.545 at which a Mach shock first appears. This agreement in the oblique wave region is consistent with the previous evidence that these waves are isentropic compressions. Below this pressure ratio the disagreement is consistent with the presence of the irreversible flow through the Mach shock wave.

Secondly it is seen that the experimental values are in agreement with the isentropic solution. This is apparently fortuitous for in both analytical solutions it is assumed that the pressure is uniform at atmospheric across the maximum diameter. The pressure distributions in Fig.12 show that this is not so, the lower pressure in the centre resulting in an enhanced Mach number there. Agreement then only occurs because of the reduced Mach number through the mixing region.

6. Jet Maximum Cross-Sectional Area

The analysis in Appendix I has also been used to calculate the maximum cross-sectional area of the jet. Values are shown plotted as the solid line in Fig.14. Also, the values are given for an isentropic jet plotted as the upper chain line. The former non-isentropic, solution is seen to be in better agreement with experimental measurements from the shadowgraph pictures. These experimental values are seen to lie below the analytical ones. The biggest discrepancy occurs at the pressure ratio of 0.545 where the Mach shock first appears. In this region there is a marked kink in the variation of the shadowgraph values.

Rayleigh (Ref.15) extended Prandlt's analysis (Ref.1) to give the shape of the jet boundary. Using the approximation made by Prandlt in deriving the previous equation for ℓ_2, Rayleigh's result can be used to give

$$\frac{A_m}{A_j} = 1 + \frac{0.54\left(\frac{p_j}{p_a} - 1\right)^2}{1 + 1.8\left(\frac{p_j}{p_a} - 1\right)}$$

Results computed from this equation agree closely with the isentropic flow solution, shown in Fig.14, for values of p_a/p_j between 0.4 and 1.0.

Results of characteristic calculations (Ref.2) are also plotted in Fig.13. They are seen to satisfy the straight line variation shown as a dash line.

Three sets of values, obtained from the traverse results given in Fig.12, are also shown plotted. They are taken as corresponding to the outer diameter of the mixing region where the Mach number is zero, as the inner edge of the linear variation of the Mach number in the mixing region, and as the inner edge of the mixing region where the slope of the Mach number distribution has a minimum value. In each of these three cases a linear variation is obtained in Fig.14.

It is seen that the viscous mixing region has a most marked effect upon the maximum cross-sectional area, thus limiting severely the value of calculations that ignore this effect such as both the present analysis and the characteristics calculations.

The slopes of these four linear variations, that is $\frac{d(A_j/A_m)}{d(p_a/p_j)}$ are respectively.

(a) For the characteristic results, 1.44*

(b) For the outer viscous zone diameter, 1.17

(c) For the intermediate viscous zone diameter, 1.67

(d) For the inner viscous zone diameter, 1.90

The corresponding slope at the origin given by the present analysis (Appendix Eqn A.6) is, for $M_j = 1.0$ and $\gamma = 1.4$,

$$\frac{d(A_j/A_m)}{d(p_a/p_j)} = 2.80$$

and so in the region of large jet pressure ratio, p_j/p_a, the present analysis gives a serious underestimate of the jet expansion.

The results shown in Fig.14 suggest that, over the lower portion of the range of p_a/p_j, there is a linear variation for A_j/A_m both for the experimental values from the traverse readings and for the numerical values obtained by the characteristics solutions. There is thus value in deriving general relations that satisfy the characteristics solution for small values of p_a/p_j. This is conveniently now done by forming comparisons with the present analysis given in Appendix I.

As indicated in Fig.15, for the range $0 \leq p_a/p_j \leq 0.1$, the results of characteristics calculations (Ref.2) can be expressed in the form,

$$(A_j/A_m) = \alpha\,(p_a/p_j) + \beta\,(p_a/p_j)^2$$

---

* This value is obtained by fitting a straight line through the three points available and so the slope is different from that given later.

which for brevity is written,

$$A_1 = \alpha P_1 + \beta P_1^2 \qquad \ldots(2)$$

and where α and β are functions of M_j and the results of Fig.15 are for $\gamma = 1.4$. Fig.15 and Eqn.(2) show that, for the characteristics results, as $P_1 \to 0$, $A_1 \propto P_1$. This is the result given by Lord (Ref.3). It disagrees with another approximate solution (Ref.16) which for $\gamma = 1.4$ gives $A_1 \propto P_1^{0.572}$

Indicating the value of $d(A_j/A_m)/d(p_a/p_j)$ for the present solution by A_2' then, from Eqn A.6, when $p_a/p_j = 0$

$$A_2' = \frac{1 + \gamma M_j^2}{M_j^2 - \frac{\gamma - 1}{2\gamma}}$$

For $1.0 \leq M_j \leq +\infty$ then correspondingly $2\gamma \geq A_2' \geq \gamma$. A comparison at common values of M_j is found to give the following results,

$$\alpha - 1 = 0.3 (A_2' - \gamma)^{\sqrt{3}}$$

and

$$\beta = - (2\gamma - A_2')^2$$

For high values of M_j for example for $M_j \geq 3$ these results give

$$\alpha = 1$$

$$\beta = - \gamma^2$$

so that from Eqn.(2)

$$A_1 = P_1 - \gamma^2 P_1^2,$$

The results of characteristic solutions that have just been used were for $\gamma = 1.4$ and so these results cannot be justified for other values of γ. For the present analysis, Eqn.A.7 shows that for $M_j = 1.0$,

$$A_2' = 2\gamma.$$

From Fig.14, the outer diameter of the jet corresponds to

$$A_2' = 1.17.$$

If this is also proportional to γ then for steam for which $\gamma = 1.2$,

$$A_2' = 1.0$$

a result that was found experimentally by Benson (Ref.17).

7. Acknowledgements

The authors are grateful to Mr. J.G. Liu and Mr. J. Rossiter for their skill in the design and manufacture of the apparatus and additionally to the former for assistance with the experimental work.

Notation

A	Cross-section area of jet
A_1	$\equiv A_j/A_m$
A_2'	$\equiv d(A_j/A_m)/d(p_a/p_j)$
A_j	Cross-section area of jet at nozzle outlet
A_m	Maximum cross-section area of jet
d_j	Diameter of jet at nozzle outlet
$J_o(x)$	Bessel function of first kind of zero order
ℓ_1	Distance to oblique shock intersection
ℓ_2	Length of first cell of jet
ℓ_3	Distance to cell maximum diameter
$\dot{m}_m$	Mass flow rate of cell maximum diameter
M_j	Jet Mach number at nozzle outlet
M_m	Jet Mach number at cell maximum diameter
n	Index (Eqn. following eqn.(1))
p	Pressure
p_o	Static pressure in settling length
p_1	Pitot pressure
p_a	Ambient pressure
p_j	Jet pressure at nozzle outlet
p_s	Stagnation pressure in settling length
P_1	$\equiv p_a/p_j$
u_j	Jet velocity at nozzle outlet
u_m	Jet velocity at cell maximum diameter
T	Jet thrust
w_1	Diameter of Mach shock
X_e	External force
X_i	Internal force

y	Radial ordinate
α	Coefficient (Eqn.2)
β	Coefficient (Eqn.2)
γ	Ratio of specific heats

References

No.	Author(s)	Title, etc.
1	L. von Prandtl	Über die stationären Wellen in einem Gasstrahl. "Physikalische Zeitschrift", Vol.5, pp 599-601, 1904.
2	E. S. Love, C. E. Grigsby, L. P. Lee and M. J. Woodling	Experimental and theoretical studies of axisymmetric free jets. NASA TR R-6: 1959.
3	W. T. Lord	On axi-symmetrical gas jets with application to rocket jet flow fields at high altitudes. ARC R & M 3235, 1959.
4	T. C. Admanson, Jr.	The structure of the rocket exhaust plume without reaction at various altitudes. "Supersonic flow, chemical process and radiative transfer". Edited by D. B. Olfe and V. Zakkay. Published for AGARD by Pergamon Press, 1964, p.177.
5	R. Ladenburg C. C. Van Voorhis and J. Winckler	Interferometric studies of faster than sound phenomena. Part II. Analysis of supersonic air jets. Phys.Rev, Vol.76, No.5, p.662, September, 1949.
6	J. Hartman and F. Lazzarus	The air jet with a velocity exceeding that of sound. Phil.Mag.Vol.31, p.35, 1941.
7	J. C. Gibbings	The combination of a contraction with a supersonic nozzle for a wind tunnel. Ingenieur Archiv. Vol. 35, p.269, 1966.
8	L. D'Attorre and F. C. Harshbarger	Parameters affecting the normal shock location in underexpanded gas jets. A.I.A.A. Jour. Vol.3, No.3, p.530, March, 1965.
9	S. Crist D. M. Sherman and D. R. Glass	Study of the highly underexpanded sonic jet. A.I.A.A. Jour. Vol.4, No.1, p.68, January, 1966.
10	L. H. Bach and R. F. Cuffel	Detection of oblique shocks in a conical nozzle with a circular-arc throat. A. I. A. A. Jour. Vol.4, No.12, p.2219, December, 1966.

11/

No.	Author(s)	Title, etc.
11	T.C. Adamson and J.A. Nicholls	On the structure of jets from highly underexpanded nozzles into still air. J.Aer.Sci. Vol.26, No.1, p.16, January 1959.
12	D. Sloan	The displacement of the nose shock wave from a pitot tube under a streamwise velocity gradient. J.R.Ae.S., Vol.71, No.682, p.725, October, 1967.
13	D.C. Pack	A note on Prandtl's formula for the wave-length of a supersonic gas jet. Quat.Jour.Mech and App. Maths, Vol.3, Pt.2, p.173, 1950.
14	R. Emden	Flow phenomena in permanent gases. Ann.d. Phys. u. Chem. Vol.69, p.426, 1899.
15	Rayleigh (Lord)	On the discharge of gases under high pressures. Phil.Mag. 6th Ser. Vol.32, P177, 1916.
16	A.F. Charwat	Boundary of underexpanded axi-symmetric jets issuing into still air. A.I.A.A. Jour. Vol.2, No.1, p.161, Jan. 1964.
17	S.F. Benson	Boiler draught production by means of the jet air-pump. Proc.I.Mech.E., Vol.153, (WEP 9), p.311, 1945.

APPENDIX

Elementary Analysis of Jet Flow

A model of the flow of an axisymmetric jet expanding from a container through a nozzle into a stationary atmosphere is shown in Fig.16. The following assumptions are made;

(a) There is no mixing of the jet with the surrounding atmosphere

(b) The pressure along the jet boundary and across section m of the jet is atmospheric

(c) The jet flow is uniform at station j and m.

A control volume, indicated I in Fig.16, is drawn to cross the jet at section m where the jet cross-sectional area reaches its first maximum value. The thrust, T, is then given by

$$T = \int u_m \, d\dot{m}_m . \qquad \ldots(A.1)$$

A second control volume is drawn around the internal surfaces of the container and across the jet at section j. Then if X_i is the force on the interior of the nozzle and container,

$$- X_i - p_j A_j = \int u_j \, d\dot{m}_j . \qquad \ldots(A.2)$$

A third control volume is drawn to contain the jet between stations j and m. Thus,

$$p_j A_j - p_m A_m + \int_j^m p \, dA = \int u_m \, d\dot{m}_m - \int u_j \, d\dot{m}_m \qquad \ldots(A.3)$$

where the integral on the left hand side is taken over the jet boundary.

The external force upon the nozzle and the container is given by,

$$X_e = p_a A_j .$$

Combining this relation with Eqs. A1 and A2 and introducing assumption (b) above, gives the total force as

$$X_i + X_e = -T$$

which indicates the feasibility of the flow model.

Introducing assumption (c) into Eqn.A.3 results in,

$$\frac{p_a}{p_j}\left[\frac{A_j}{A_m} + \gamma M_m^2\right] = \frac{A_j}{A_m}\left[1 + \gamma M_j^2\right] . \qquad \ldots(A.4)$$

Using assumption (a), the equation of continuity gives,

$$\frac{A_j}{A_m} = \frac{M_m}{M_j}\frac{p_a}{p_j}\left[\frac{1 + \frac{\gamma - 1}{2} M_m^2}{1 + \frac{\gamma - 1}{2} M_j^2}\right]^{\frac{1}{2}} \qquad \ldots(A.5)$$

Thus Eqns. A.4 and A.5 are simultaneous ones giving solutions for A_j/A_m and M_m in terms of p_a/p_j and M_j.

When $p_a/p_j \to 0$, then $A_j/A_m \to 0$ and then from Eqn. A.4

$$\frac{p_a/p_j}{A_j/A_m} \to \frac{1 + \gamma M_j^2}{\gamma M_m^2}$$

whilst from Eqn.A.5

$$\frac{p_a/p_j}{A_j/A_m} \to \frac{M_j}{M_m}\left[\frac{1 + \frac{\gamma - 1}{2} M_j^2}{1 + \frac{\gamma - 1}{2} M_m^2}\right]^{\frac{1}{2}} .$$

Equating those two relations gives,

$$M_m^2 \to \frac{(1 + \gamma M_j^2)^2}{\gamma M_j^2 - \frac{\gamma - 1}{2}}$$

whilst substitution of this in turn gives,

$$\frac{p_a/p_j}{A_j/A_m} \to \frac{M_j^2 - \frac{\gamma - 1}{2\gamma}}{1 + \gamma M_j^2} . \qquad \ldots(A.6)$$

For $M_j = 1$ these last two relations give

$$M_m^2 = 2(\gamma + 1)$$

and

$$\frac{P_a/P_j}{A_j/A_m} = \frac{1}{2\gamma} \quad . \qquad \ldots(A.7)$$

Whilst as $M_j \to \infty$

$$M_m^2/M_j^2 \to \gamma$$

and

$$\frac{P_a/P_j}{A_j/A_m} \to \frac{1}{\gamma} \quad .$$

30371
FIGS 1 & 2

FIG. 1

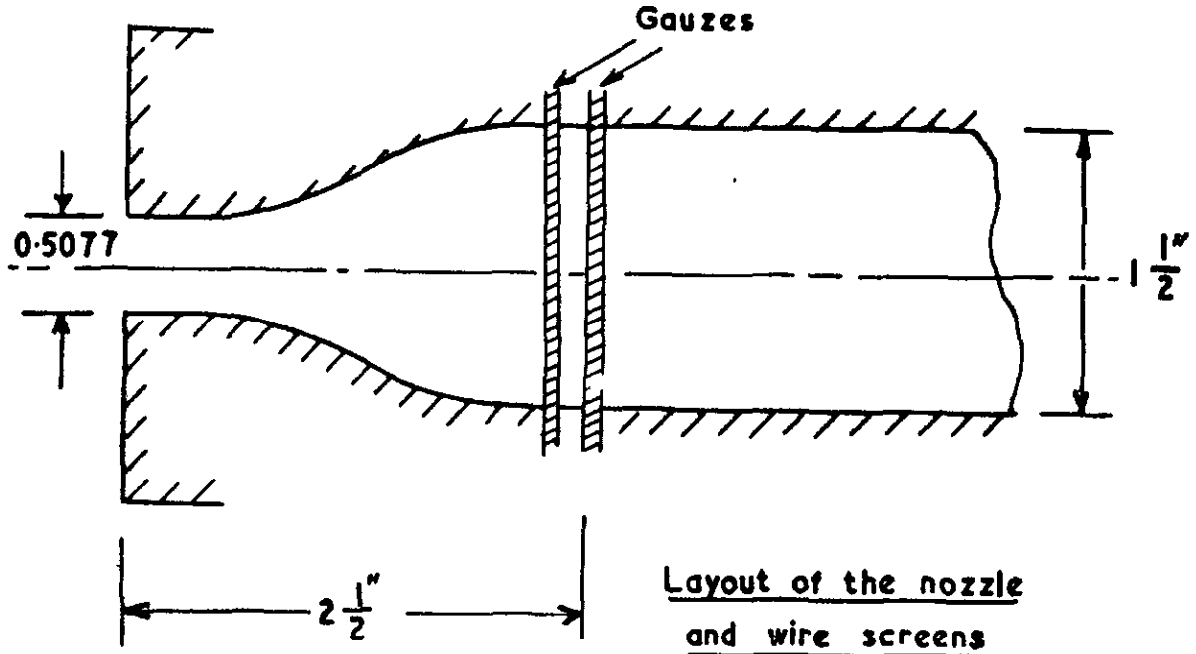

Layout of the nozzle and wire screens

FIG. 2

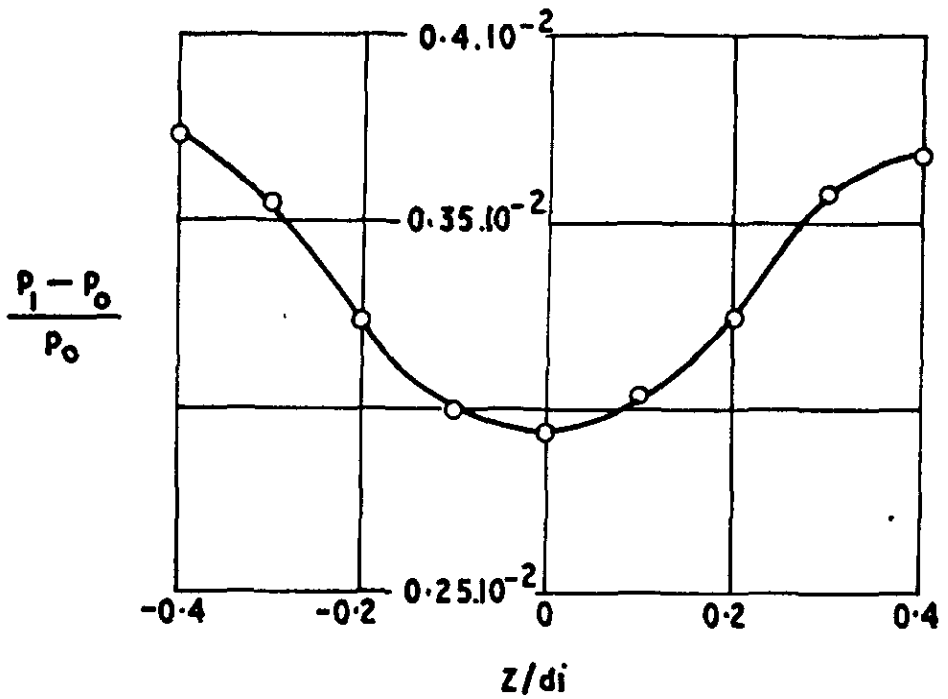

Distribution of total pressure at the nozzle outlet

30371
FIG. 3

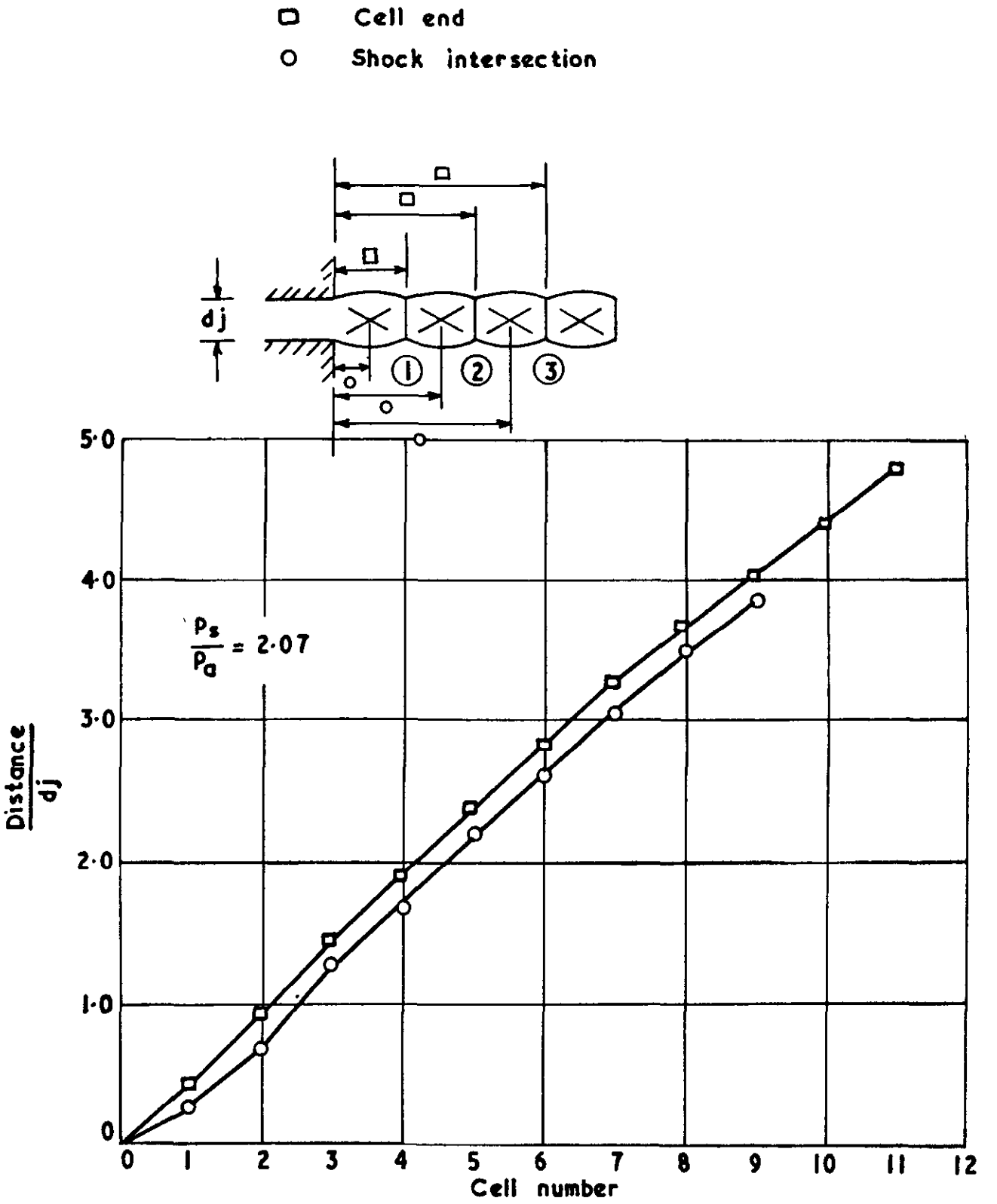

Distances to the cell ends and the shock intersections

30371
FIG.4

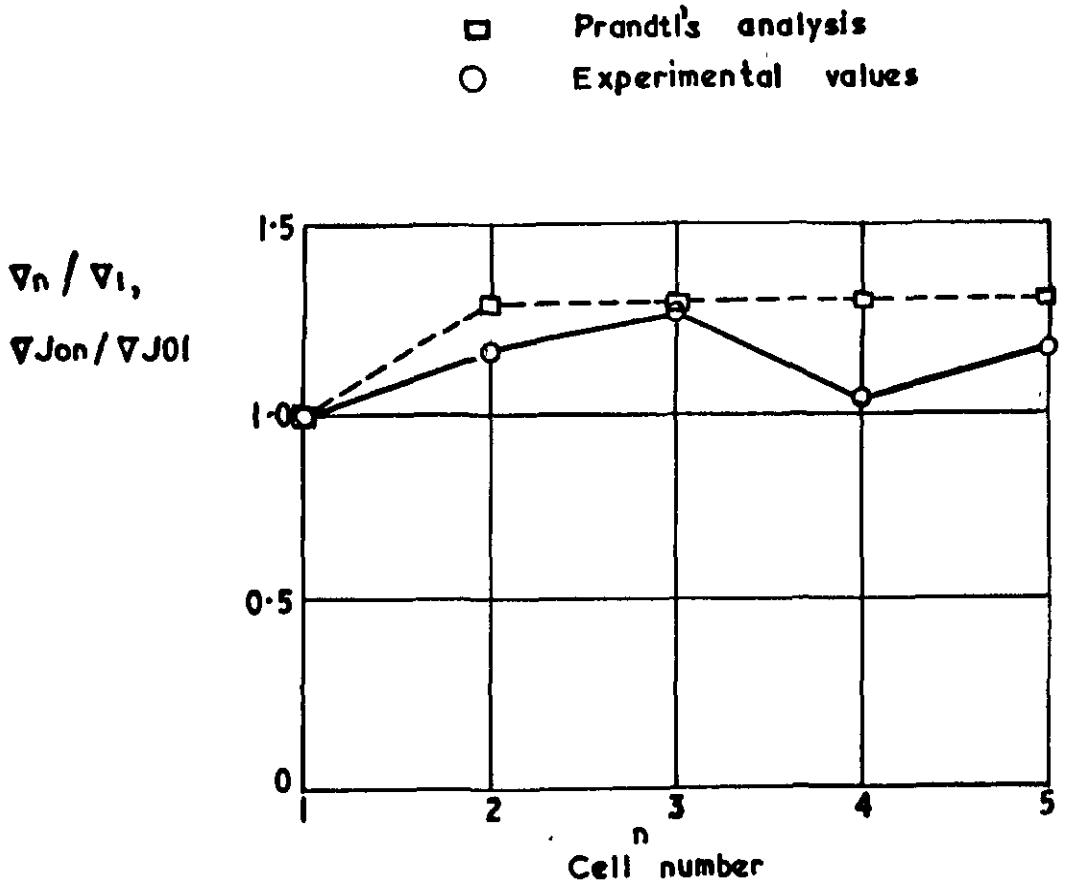

Cell lengths

30 371
FIG. 5

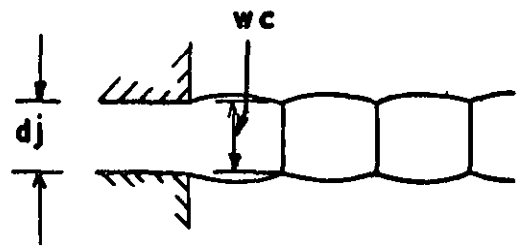

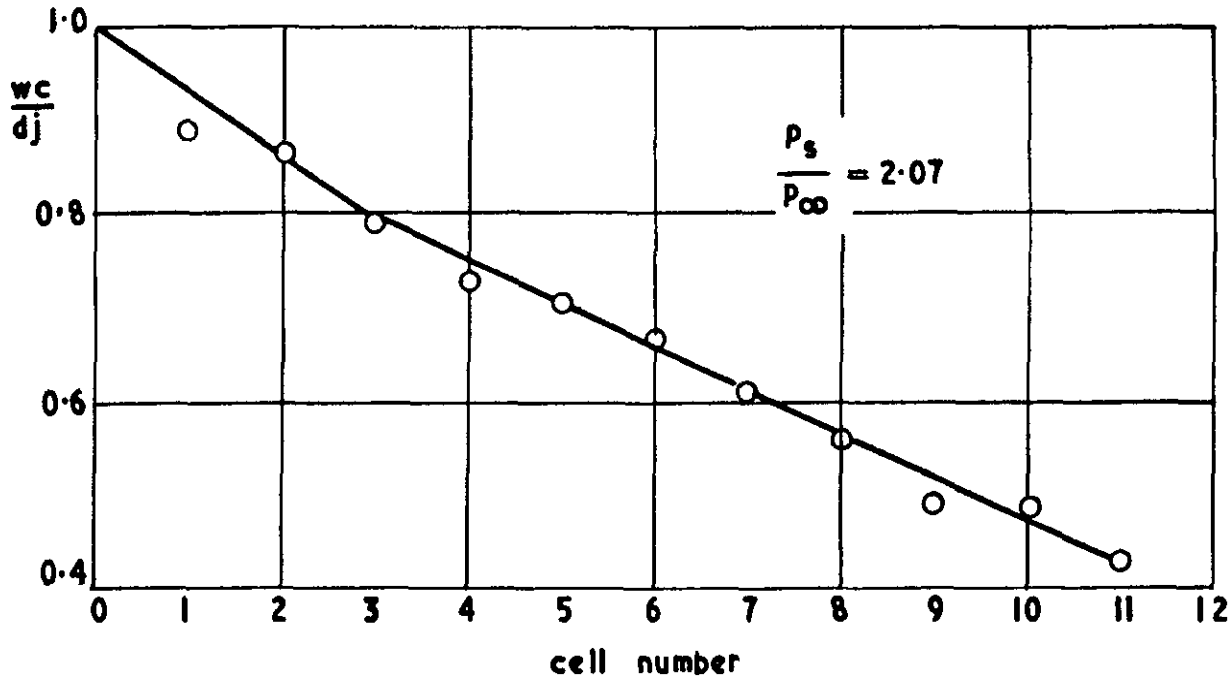

Width of cell joints

30371
FIG.6

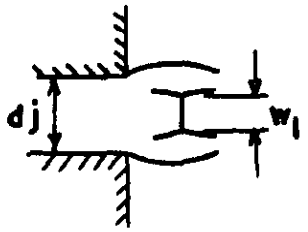

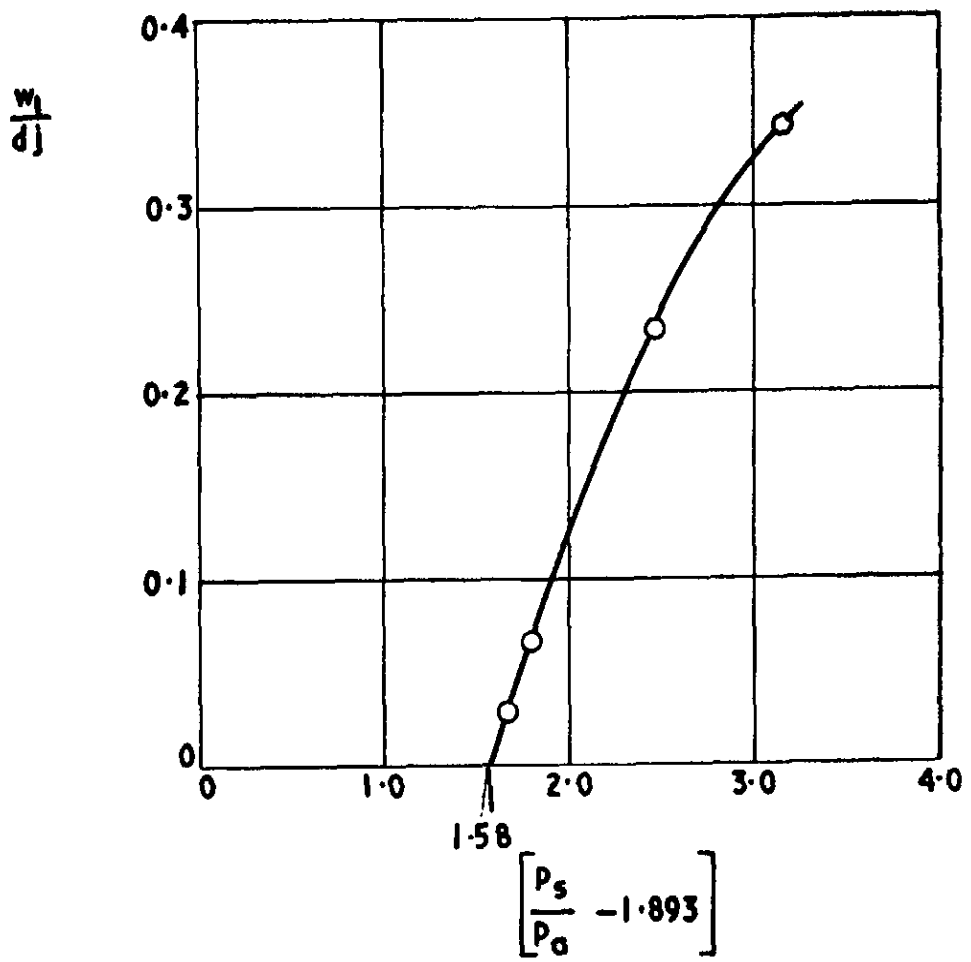

Width of Mach shock

30371
FIG. 7

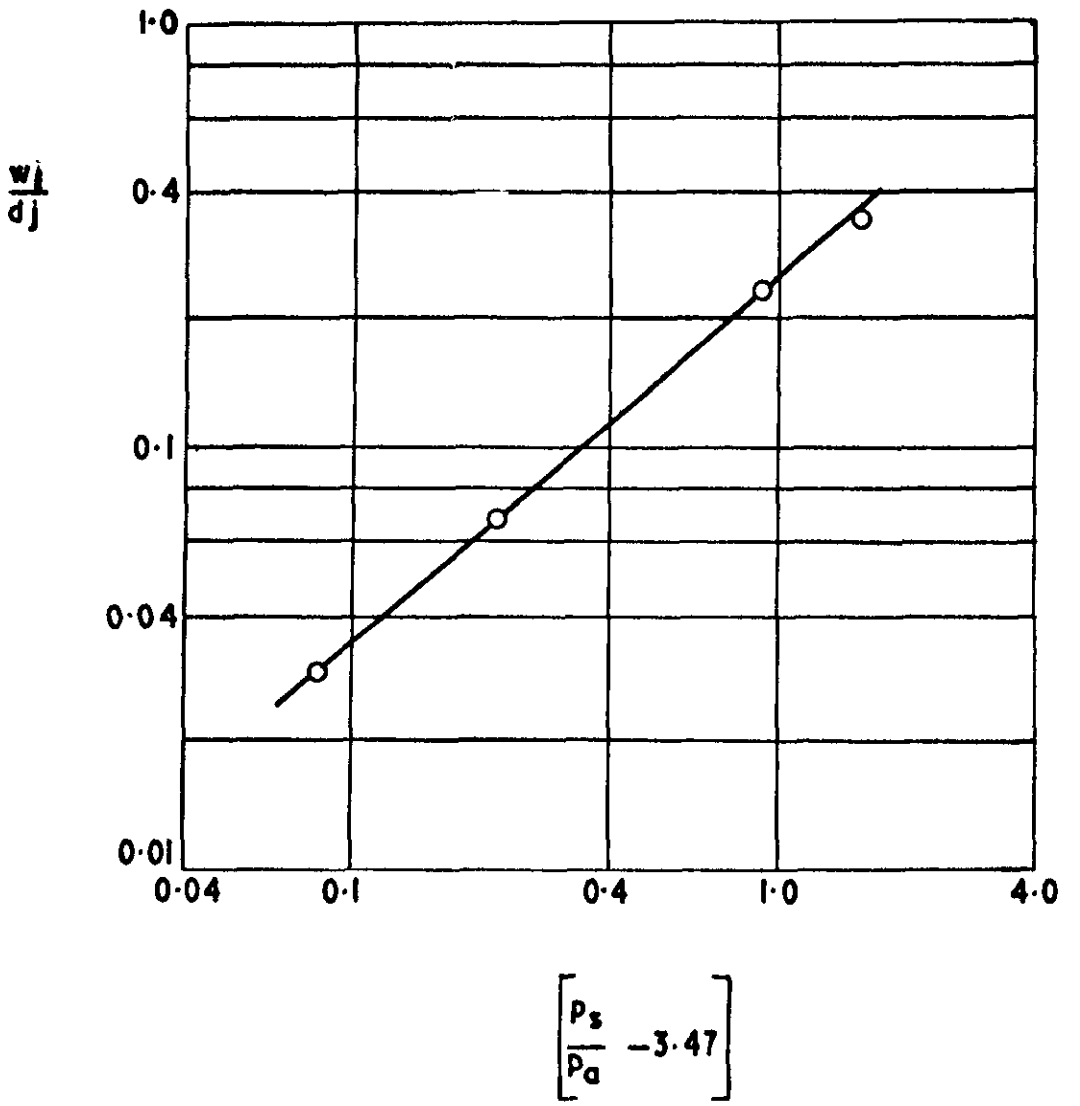

Width of Mach shock

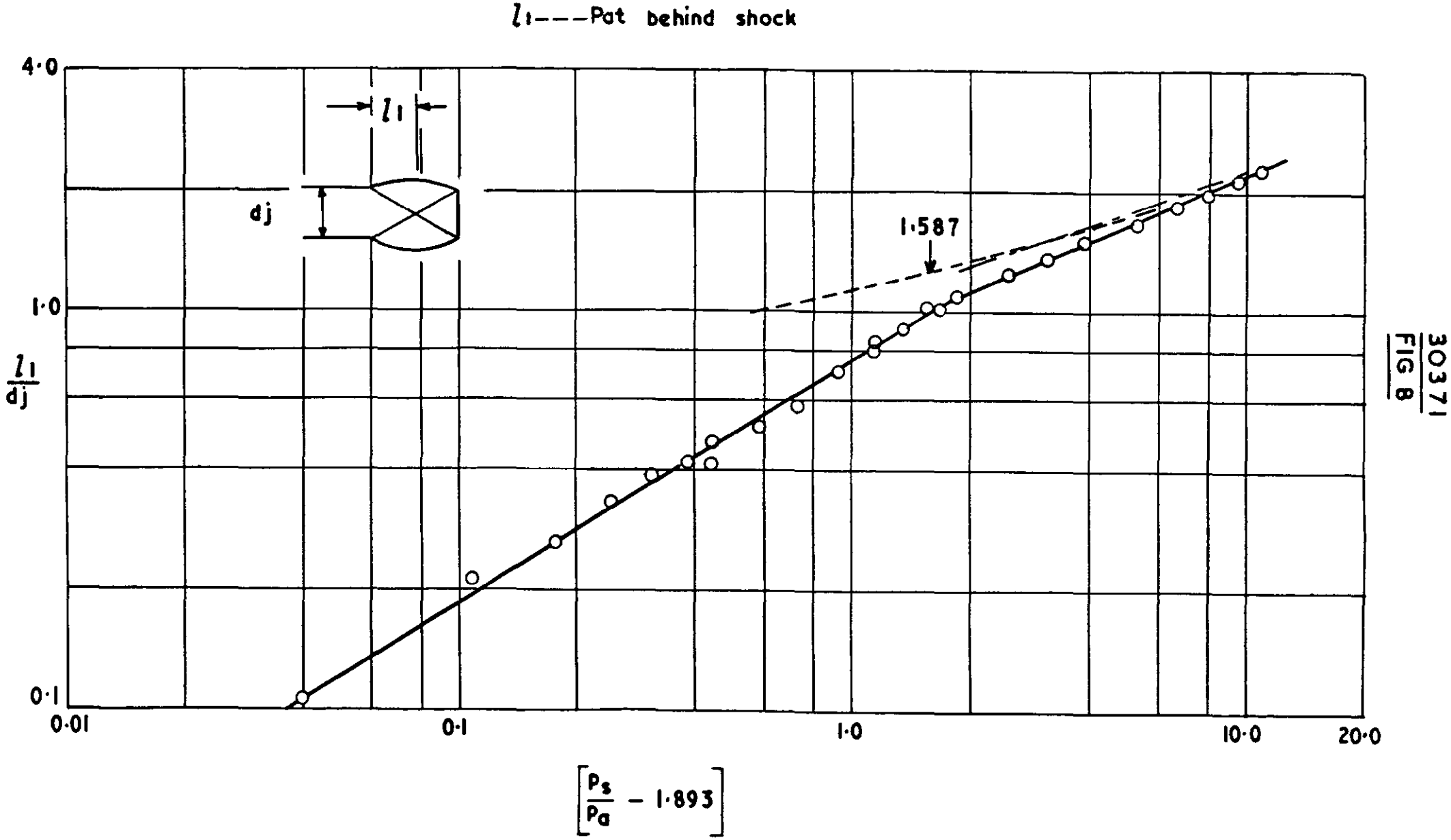

30371
FIG 8

Distance to the first shock intersection with the axis

30371
FIG.9

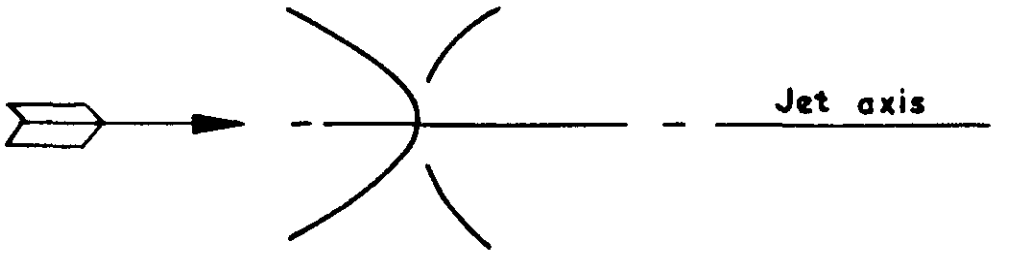

Scale
0 1 In.

Shadowgraph of shock intersection

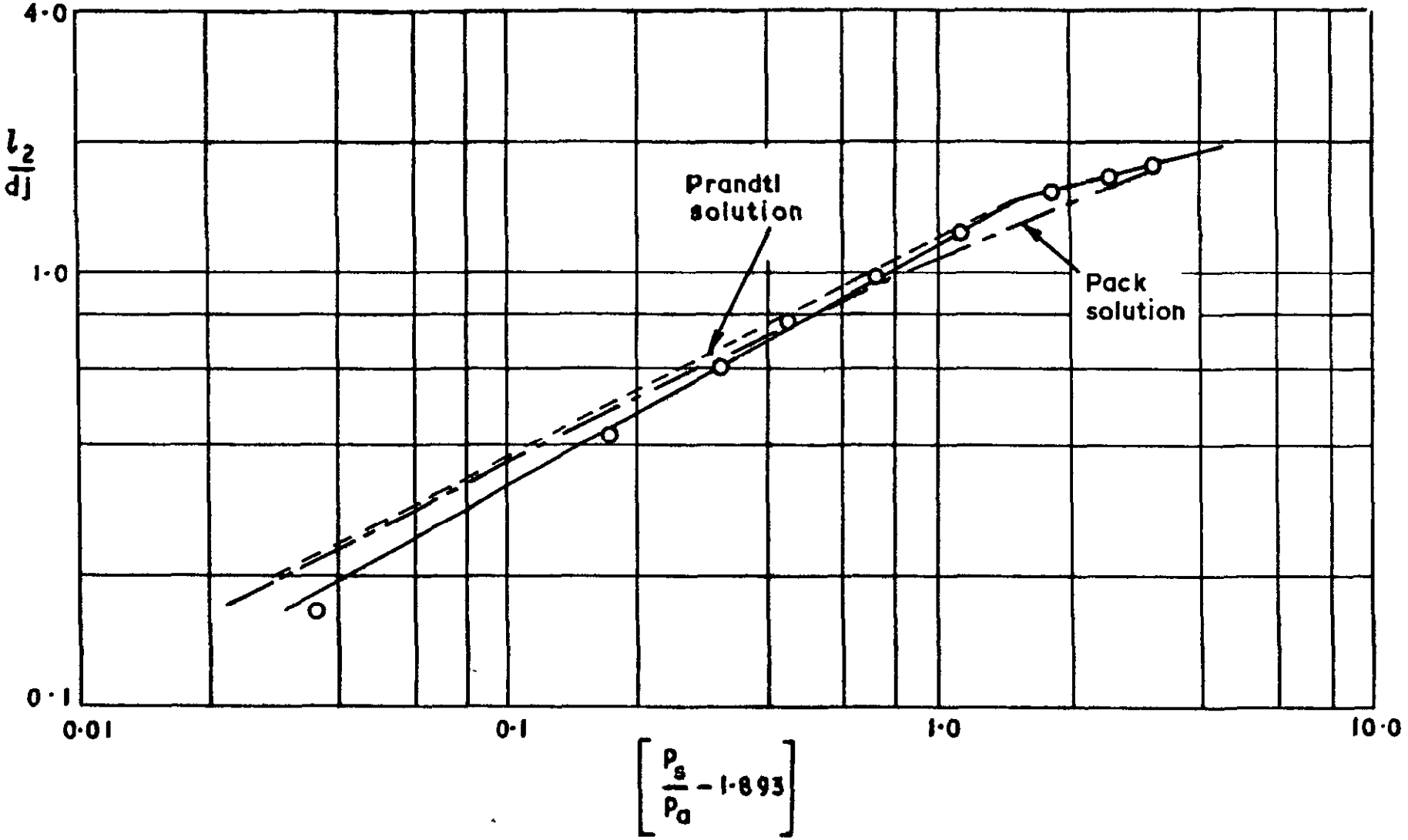

30371
FIG. 10

Length of the first cell

30371
FIG. 11

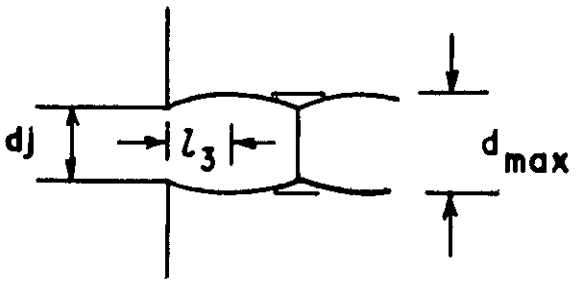

O Shadowgraph

Δ Characteristics

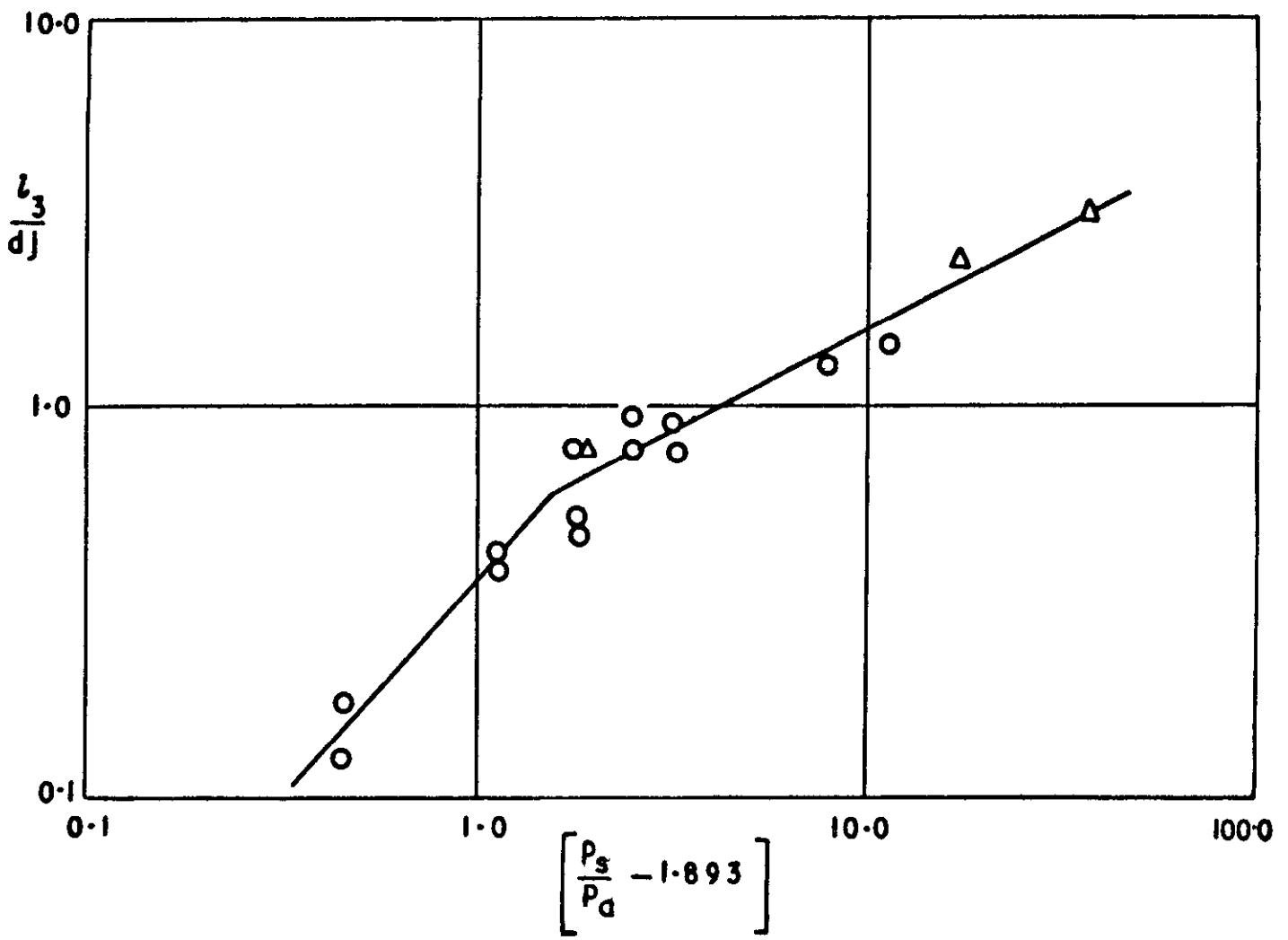

Distance to the first maximum diameter

30371
FIG.12a

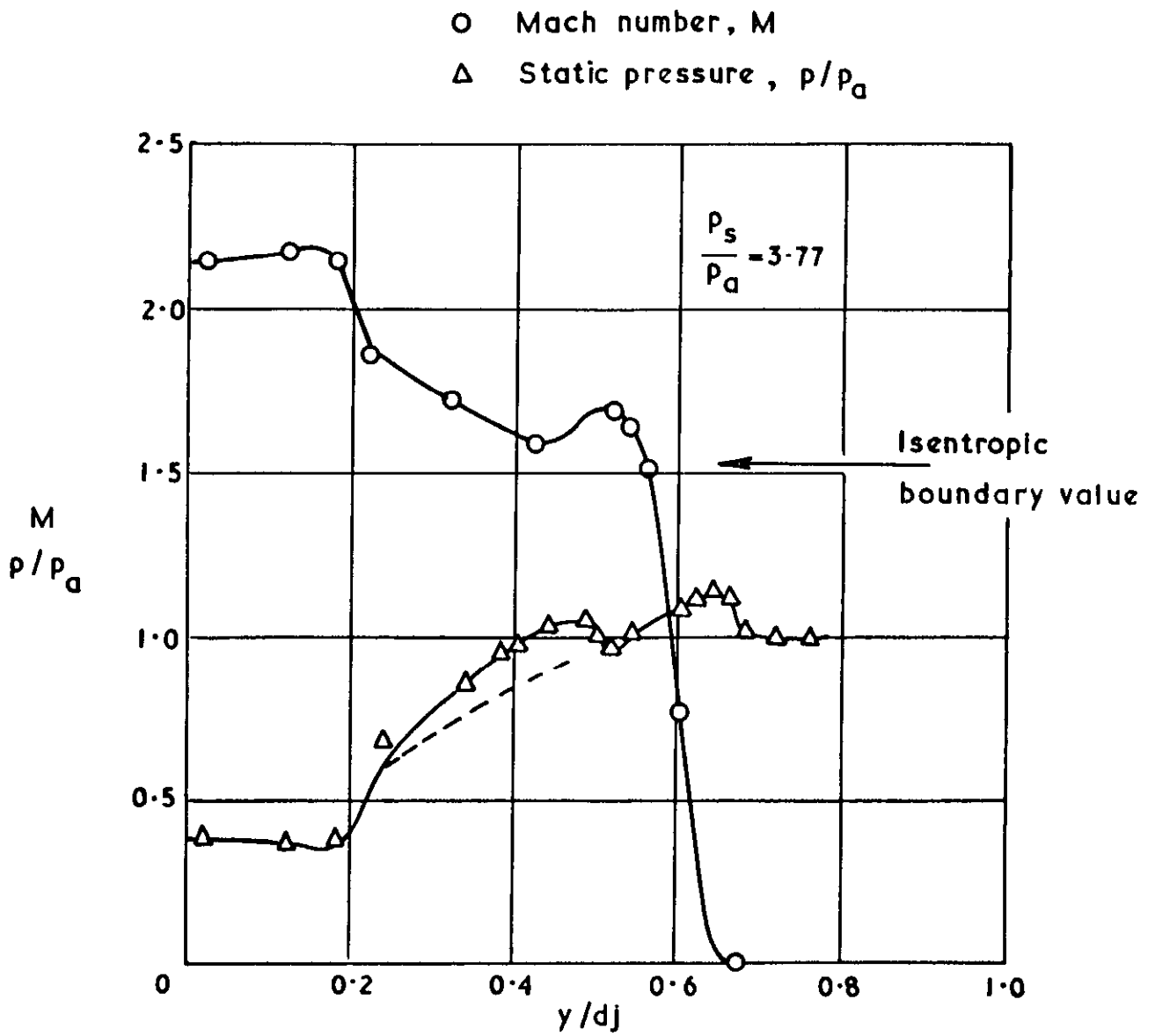

Mach number and static pressure distribution across the first maximum diameter of the jet

30 371
FIG. 12 b

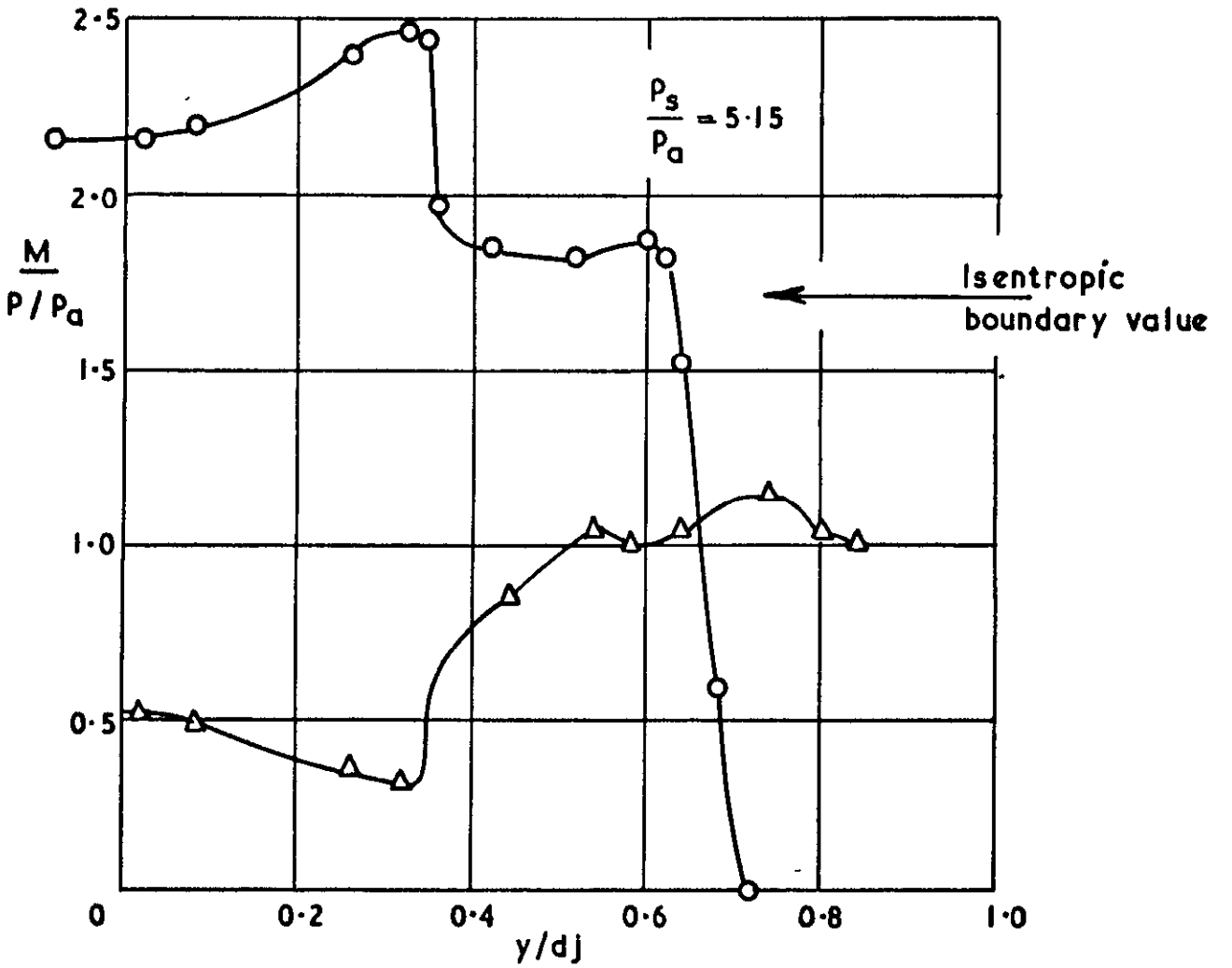

Mach number and static pressure distribution across the first maximum diameter of the jet

30 371
FIG. 12c

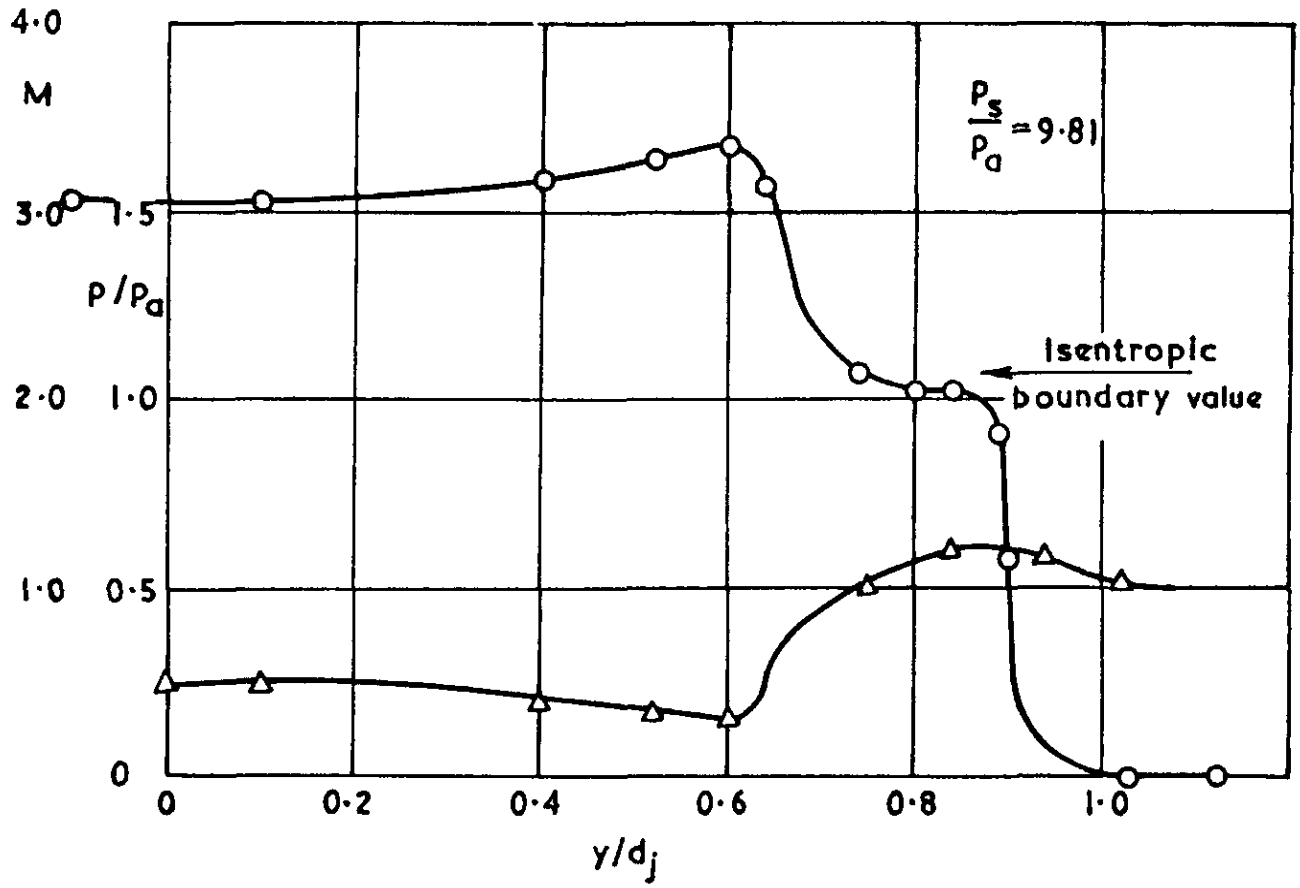

Mach number and static pressure distribution across the first maximum diameter of the jet

30 371
FIG. 12d

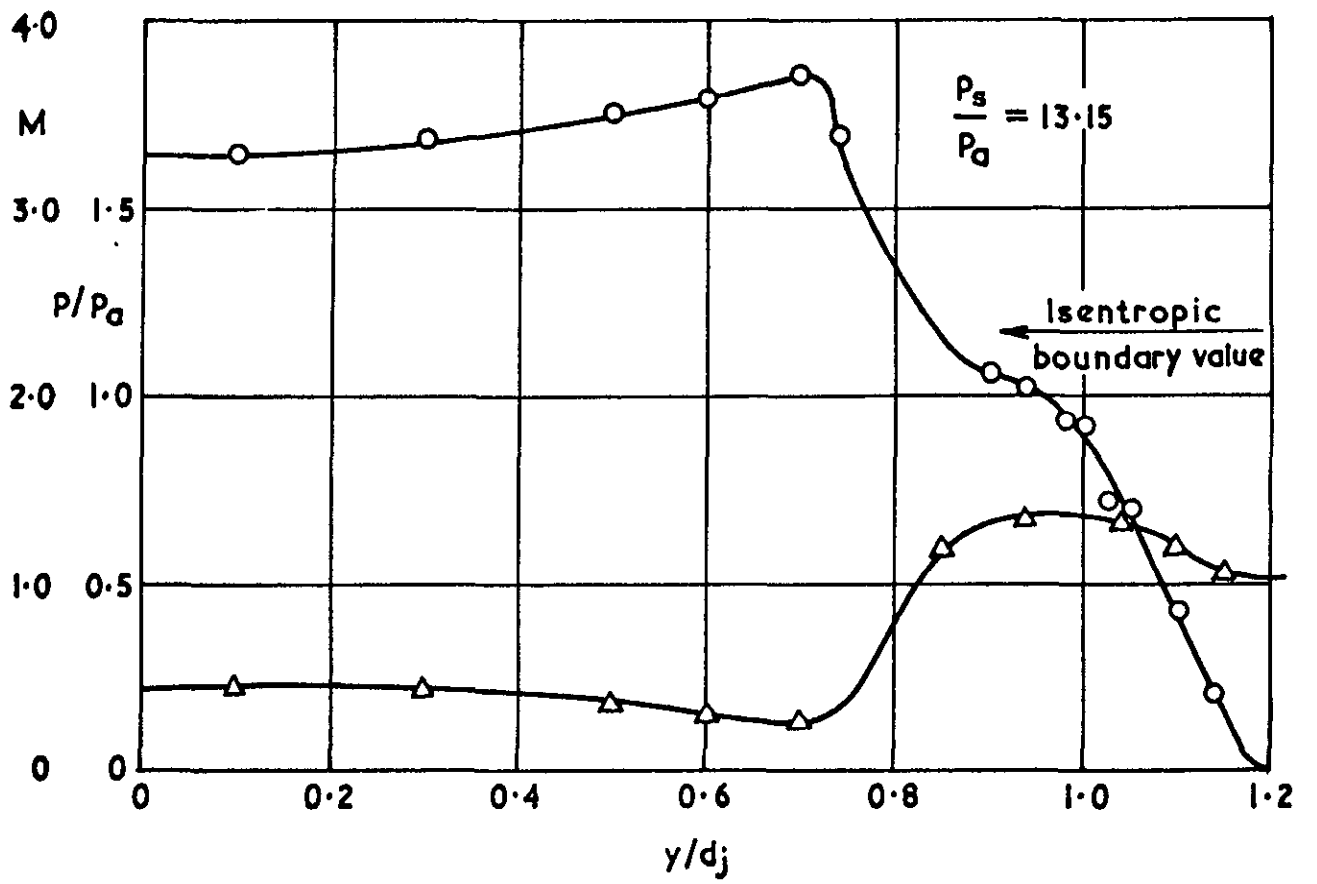

Mach number and static pressure distribution across the first maximum diameter of the jet

30 371
FIG. 13

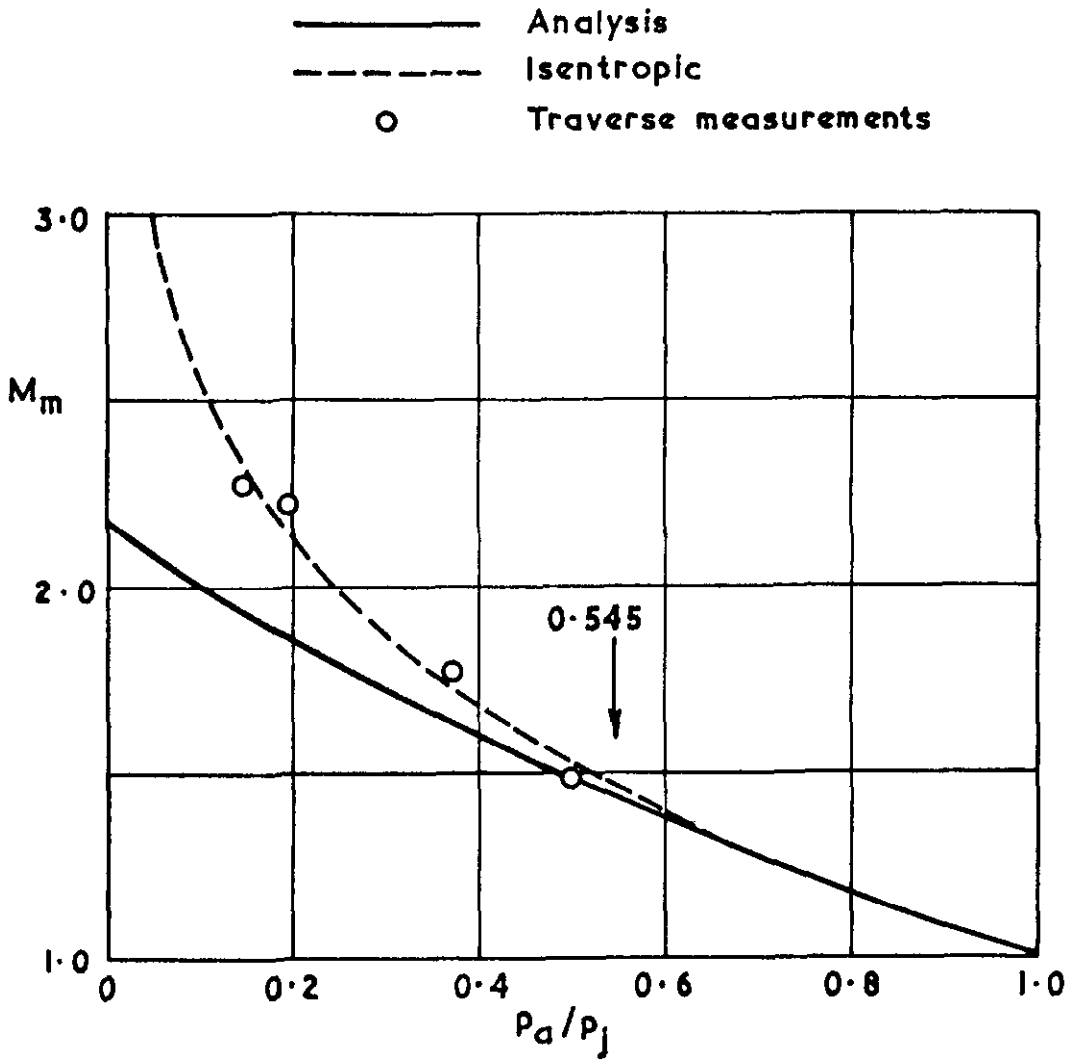

Mean Mach number

30 371
FIG. 14.

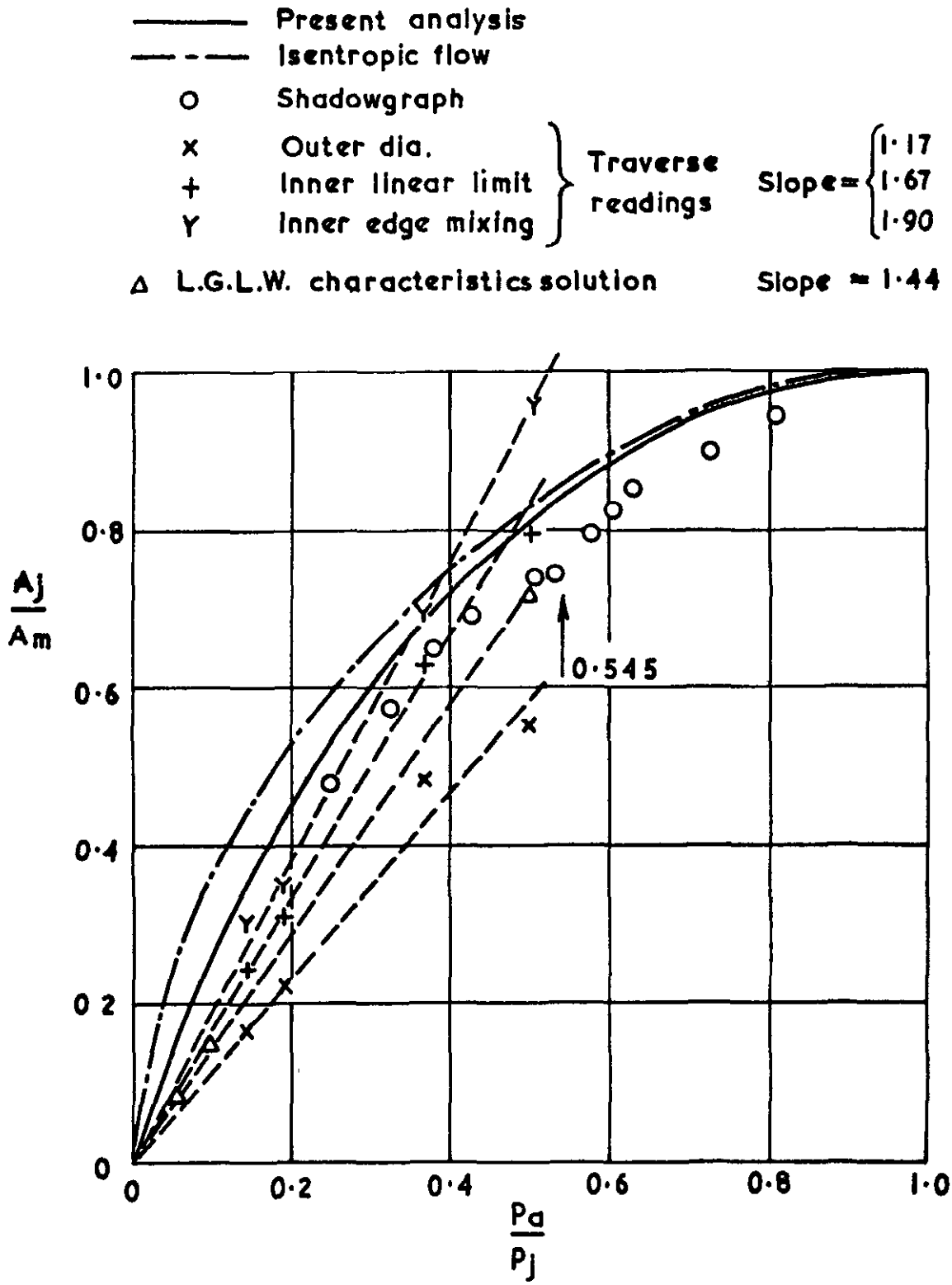

Cross-sectional area at the first maximum diameter

30371
FIGS. 15 & 16

FIG. 15

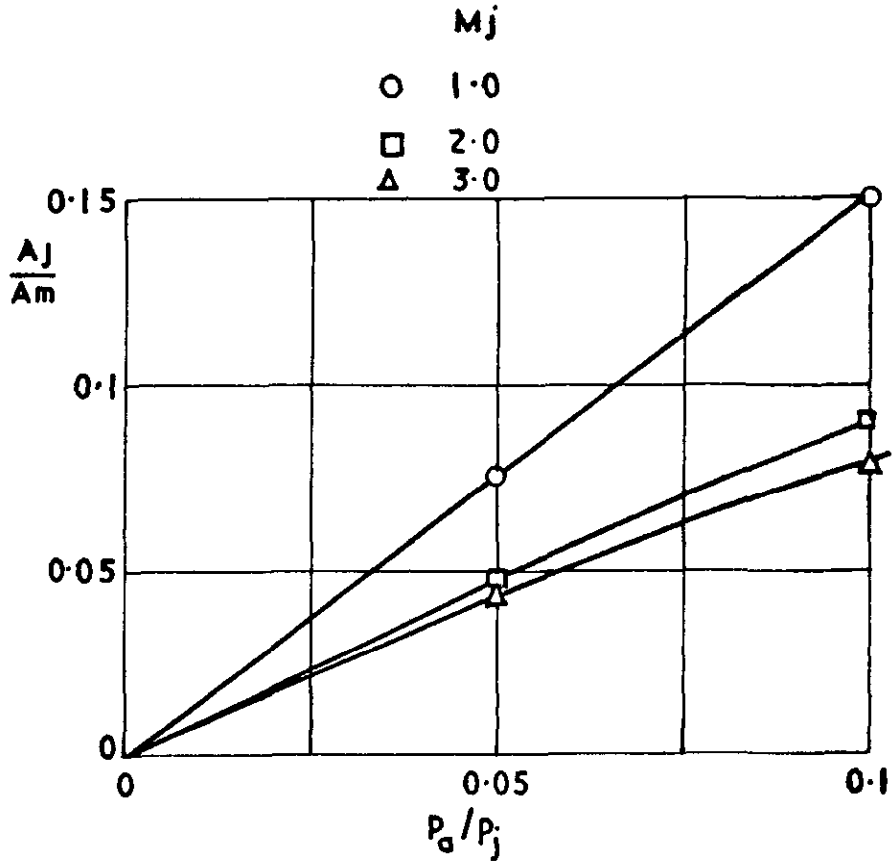

Cross-sectional area at the first maximum diameter
Ref 2

FIG. 16

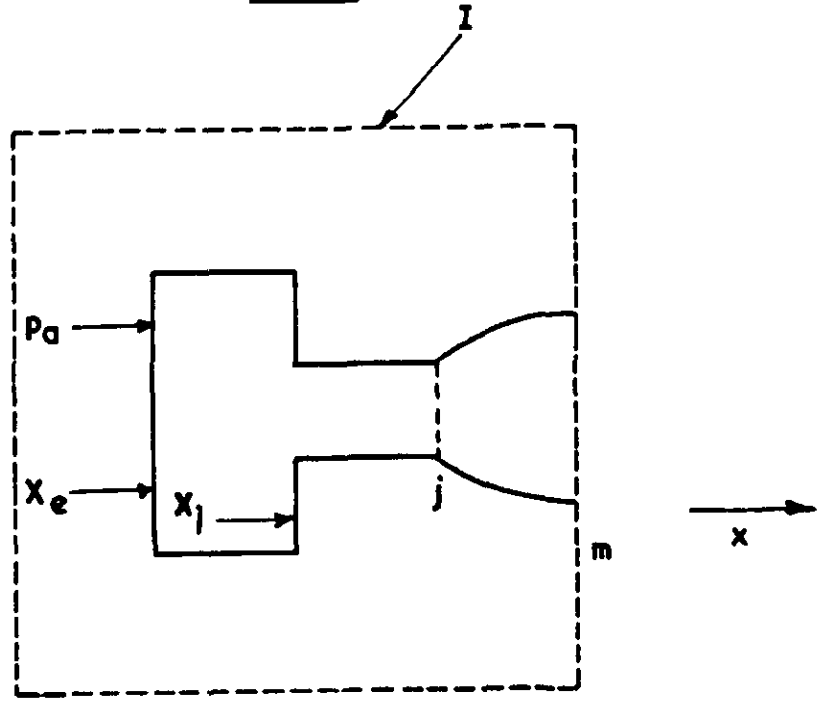

Control volumes for the jet flow

Produced and published by
HER MAJESTY'S STATIONERY OFFICE

To be purchased from
49 High Holborn, London WC1V 6HB
13a Castle Street, Edinburgh EH2 3AR
109 St Mary Street, Cardiff CF1 1JW
Brazennose Street, Manchester M60 8AS
50 Fairfax Street, Bristol BS1 3DE
258 Broad Street, Birmingham B1 2HE
80 Chichester Street, Belfast BT1 4JY
or through booksellers

Printed in England

C.P. No. 1197

SBN 11 470465 1

and

$$\frac{p_a/p_j}{A_j/A_m} = \frac{1}{2\gamma} \quad . \qquad \ldots(A.7)$$

Whilst as $M_j \to \infty$

$$M_m^2/M_j^2 \to \gamma$$

and

$$\frac{p_a/p_j}{A_j/A_m} \to \frac{1}{\gamma} \quad .$$